Title

Characterisation of impaired wound healing in a preclinical model of induced diabetes using wide-field imaging and conventional immunohistochemistry assays

Journal

International Wound Journal, 16(1)

ISSN

1742-4801

Authors

Saidian, Mayer
Lakey, Jonathan RT
Ponticorvo, Adrien
et al.

Publication Date

2019-02-01

DOI

10.1111/iwj.13005

Peer reviewed

Characterisation of impaired wound healing in a preclinical model of induced diabetes using wide-field imaging and conventional immunohistochemistry assays

Mayer Saidian[1,2] | Jonathan R.T. Lakey[3] | Adrien Ponticorvo[2] | Rebecca Rowland[2] | Melissa Baldado[2] | Joshua Williams[2] | Maaikee Pronda[2] | Michael Alexander[3] | Antonio Flores[3] | Li Shiri3 | Stellar Zhang[3] | Bernard Choi[2,4,5] | Roni Kohen1 | Bruce J. Tromberg[2,4] | Anthony J. Durkin[2,4]

Major complications of diabetes lead to inflammation and oxidative stress, delayed wound healing, and persistent ulcers. The high morbidity, mortality rate, and associated costs of management suggest a need for non-invasive methods that will enable the early detection of at-risk tissue. We have compared the wound-healing process that occurs in streptozotocin (STZ)-treated diabetic rats with non-diabetic controls using contrast changes in colour photography (ie, Weber Contrast) and the non-invasive optical method Spatial Frequency Domain Imaging (SFDI). This technology can be used to quantify the structural and metabolic properties of invivo tissue by measuring oxyhaemoglobin concentration (HbO2), deoxyhaemoglobin concentration (Hb), and oxygen saturation (StO2) within the visible boundaries of each wound. We also evaluated the changes in inducible nitric oxide synthase (iNOS) in the dermis using immunohistochemistry. Contrast changes in colour photographs showed that diabetic rats healed at a slower rate in comparison with non-diabetic control, with the most significant change occurring at 7 days after the punch biopsy. We observed lower HbO2, StO2, and elevated Hb concentrations in the diabetic wounds. The iNOS level was higher in the dermis of the diabetic rats compared with the non-diabetic rats. Our results showed that, in diabetes, there is higher level of iNOS that can lead to an observed reduction in HbO_2 levels. iNOS is linked to increased inflammation, leading to prolonged wound healing. Our results suggest that SFDI has potential as a non-invasive assessment of markers of wound-healing impairment.

[1]The Institute for Drug Research, School of Pharmacy, The Hebrew University of Jerusalem, Jerusalem, Israel
[2]Beckman Laser Institute and Medical Clinic, University of California Irvine, Irvine, California
[3]Department of Surgery, University of California Irvine, Orange, California
[4]Department of Biomedical Engineering, University of California Irvine, Irvine, California
[5]Edwards Life Sciences Center for Advanced Cardiovascular Technology, University of California Irvine, Irvine, California

Correspondence
Mayer Saidian, PhD, Beckman Laser Institute and Medical Clinic, 1002 Health Sciences Road East, Irvine, CA 92617. Email: msaidian@uci.edu

1 | INTRODUCTION

Diabetes is a worldwide epidemic, affecting almost 194 million people, including 20.8 million in the United States.[1] A main cause for hospital admissions for diabetic patients is morbidity related to foot ulcers,[2] where 15% of diabetic patients suffer foot ulcers,2 of which 84% will progress to lower-leg amputations.[3] A principal cause of foot ulcers is delayed wound healing4 that was not caught clinically.

Wound healing occurs in four major phases: haemostasis, inflammation, proliferation, and remodelling.[5] Haemostasis includes the formation of a temporary matrix, secretion of cytokines and other growth factors, and interaction of cytokines with extracellular matrix (ECM), initiating the repair process.[6,7] Neutrophils initiate the following inflammatory phase, in which bacteria and debris are cleansed from the wound area. Cytokines and growth factors are released, which recruit and activate fibroblasts and epithelial cells, creating conditions for initiating the proliferative phase.[8–10] In the presence of newly formed blood vessels, fibroblasts proliferate and synthesise ECM components. Endothelial cells proliferate and migrate above the granulation tissue, causing "closure" of the wound surface.[6,11] During the remodelling phase, there is a depletion of fibroblasts and a reduction in vascular density. A matrix-resembling dermis, including mature, cross-linked collagen fibres, will create the structure of the newly formed tissue.[6]

In patients with diabetes, there is a delay in the delivery of inflammatory cells into the wounded site.[12] As the cells establish themselves in the wounds, there is also prolonged and chronic inflammation, preventing the deposition of matrix components, remodelling, and closure of the wound.[13] In this manuscript, we will focus on two biomarkers of inflammation and delayed wound healing: inducible nitric oxide synthase (iNOS) and oxygen consumption.

1.1 | Inducible nitric oxide synthase

Most cell types can produce nitric oxide (NO). Production of NO is accomplished by three distinct isoforms of nitric oxide synthases (NOS): neuronal (nNOS), inducible (iNOS), and endothelial (eNOS).[14] Under hyperglycaemic conditions, oxidative stress activates nuclear factor-κB (NF-κB),[15] leading to the upregulation of pro-inflammatory factor iNOS,[16,17] While NO has an important role related to endothelial function, the iNOS-catalysed overproduction of NO is cytotoxic,[16] leading to the formation of peroxynitrite, causing cell toxicity[18] and leading to delayed wound healing.[19]

1.2 | Oxygen in wound healing

Oxygen is crucial for wound healing, contributing to cellular adenosine triphosphate (ATP) production through mitochondrial oxidative phosphorylation.[20] ATP provides energy for cell function and protein synthesis.[21] During the inflammatory phase, oxidant levels increase via Nicotinamide adenine dinucleotide phosphate (NADPH)-linked oxygenase, consuming high amounts of oxygen,[22] and oxygen limitation can prolong the inflammatory phase. Molecular oxygen is also necessary for collagen synthesis during the remodeling phase.[23]

Diabetic hyperglycaemia can negatively affect the microvasculature by causing endothelial cell damage, causing abnormal vascular function, reducing perfusion, and decreasing oxygen and nutrient delivery to the wound.24 As such, the ability to monitor parameters related to tissue oxygenation has the potential utility to non-invasively assess healing.

There are several optical methods that have been developed for monitoring in-vivo oxygen saturation (StO2). Spectrophotometric intracutaneous analysis (SIAscope) evaluates burn wounds by calculating haemoglobin and melanin maps based on spectral analysis of back-reflected light. Similarly, hyperspectral imaging25 uses wavelengths between 500 and 700 nm to provide information on oxygenated haemoglobin (HbO_2) and deoxygenated haemoglobin (Hb) in burn and diabetic wounds, creating anatomical tissue StO_2 maps that may predict the risk of ulceration in the diabetic foot before it occurs.[26] In our case, we use spatial frequency domain imaging (SFDI), which has been used to examine reconstructive surgery,[27] port wine stain response to therapy,[28] and burn wound severity assessment.[29,30] In this study, SFDI was used to evaluate the macroscopic changes in HbO_2, Hb, and StO_2 within wounds in normal versus streptozotocin (STZ) diabetic animals and then combining this observation with NF-κB and iNOS expression analysis.

2 | MATERIALS AND METHODS

2.1 | Animals

We used 9- to 10-week-old CD hairless rats (a spontaneous mutation model of rat isolated from a Crl:CD(SD) colony in Charles River Laboratories Inc., San Diego, California, n = 9). These rats have a normal immune system but phenotypically minimal hair, obviating the need for repeated depilation.31 Six rats received an intraperitoneal (IP) injection of 65 mg/kg STZ (Enzo Lifesciences, Farmingdale, NY, USA) to induce diabetes.[32] After confirmation of diabetes (blood glucose > 350 mg/dL for three consecutive days), rats received a slow-release insulin implant (Linshin Canada, Inc. Toronto, Ontario, Canada) to control blood glucose within 200 to 400 mg/dL. Insulin was given to prevent hyperglycaemic weight loss. Rats losing 20% or more of their initial body weight were sacrificed in compliance with The Institutional Animal Care and Use Committee (IACUC) protocol. Non-diabetic rats received an IP injection of saline. Depilation cream was topically applied to the dorsal side of each rat (Nair, Church and Dwight, Princeton, New Jersey) 3 days before imaging began. Prior to the experiment, animals were placed in a custom plexiglass chamber for administration of 2% to 5% isoflurane gas. For imaging and biopsy, 2% isoflurane was administered using a nose cone. At the completion of imaging day 28, rats were euthanised with an IP injection of sodium pentobarbital (150 mg/kg).

2.2 | Excision wound model in rats

A round, full-thickness excision wound of 4.0 mm in diameter and 2 mm depth was produced in the dorsal skin by picking up a skinfold at the midline and using a sterile

disposable AcuPunch (Acuderm Inc., Fort Lauderdale, Florida). The wound-healing process was followed for 28 days (Figure 1).

For diabetic rats, each wound was created 2 weeks after the rats were considered to be diabetic, with blood glucose of >350 mg/dL. In non-diabetic rats, each wound was created 2 weeks after the saline injection.

2.3 | Evaluating wound healing using colour photography and Weber contrast

After creating wounds, we recorded colour images on each day of wound healing in a fixed geometry, using a 14-megapixel digital camera (NEX-3, Sony Corporation of America, New York, New York). Images were taken after each SFDI measurement31 on days 0 (post-wound creation), 2, 4, 7, 9, 14, 16, 21, 23, and 28 after the wound was created.[33] We quantified the difference in colour between the wounded and non-wounded area using Weber contrast, defined as follows[34]:

$$C = \frac{\Delta I}{I} = \frac{I_{\mathrm{ROI}} - I_{\mathrm{Background}}}{I_{\mathrm{Background}}}. \qquad (1)$$

Weber contrast enables the quantitative comparison of a region of interest (such as a wound) to its surroundings.[35] In our study, IROI is the average pixel intensity of the imaged punch-wound area, and $I_{\mathrm{Background}}$ is the average pixel intensity of its non-wounded surroundings. Images acquired were imported into MATLAB and grayscaled.[36] We determined the wounded region of interest by first performing a Gaussian blur, $\sigma = 2$, and thresholding the image based on the 95-percentile intensity in order to segment approximately 5 % of the pixels in frame.[37] We calculated IROI as the average intensity of the thresholded region and IBackground as the average of the non-thresholded region for Equation (1). At each time point, we calculated and compared contrast values between both groups as the wound healed.

2.4 | Spatial frequency domain imaging

SFDI provides quantitative two-dimensional mapping of subsurface tissue chromophore concentrations, including HbO_2 and Hb. Based on these values, it calculates the StO_2 values.[28,30,38–40] More details on SFDI instrumentation can be found in the literature.[31,41,42] Briefly, a 250 W quartztungsten lamp (Newport Oriel, Stratford, Connecticut) coupled to a digital micromirror device (DMD) (Texas Instruments, Dallas, Texas) projects a series of sinusoidal intensity patterns onto a 90 × 66 mm field of view. Five spatial frequency patterns equally spaced from 0 to 0.2 mm^{-1} were projected onto the illumination field, and reflected light from the sample was captured by Charged Coupled Device (CCD) camera (Nuance, CRI, Inc., Woburn, Massachusetts) with a liquid-crystal tunable filter (λ = 650-1100 nm, FWHM = 10 nm). This system was used to collect images at 17 equally spaced wavelengths between 650 and 970 nm. Data were calibrated to a reference phantom having known optical properties.[43,44] MATLAB (MathWorks, Inc., Natick, Massachusetts) was used to process the data.[42]

At each wavelength, optical properties (reduced scattering and absorption coefficients) of the measured tissue were determined by fitting the collected reflectance

data to a lookup table for scattering and absorption at both spatial frequencies generated by forward Monte Carlo simulations.[45] A linear least-squares fit algorithm was used to transform the absorption coefficient values into concentration of HbO2 and Hb using Beer's law. We used the absorption maps of estimated chromophore concentration maps of oxygenated and deoxygenated area and then converted them to tissue oxygenation (StO2) by dividing oxygenated haemoglobin by the sum of oxygenated and deoxygenated haemoglobin. The region of interest for SFDI imaging was consistently chosen to be 4 mm × 4 mm at each time point to match the size of the punch biopsy and the colour images.

2.5 | Immunofluorescent staining for evaluation of Inos

We evaluated iNOS expression at three time points by taking skin biopsies in all animals, performed 2 weeks after induction of diabetes in non-control animals. In each case, the biopsy site used was the wound area of interest. The last set of biopsies was taken 28 days after the creation of the wound, prior to sacrificing each rat.

Supplies include Tris-buffered saline solution with 0.05% Tween-20 (TBST, Sigma Aldrich St. Louis, Missouri); Insta-pot IP-LUX pressure cooker (Instant Pot Company, Ottawa, Ontario, Canada); protein block and anti-iNOS; secondary antibodies (Abcam, Cambridge, Massachusetts), formalin, Sudan black, and DAPI (Thermo Fisher Scientific, Waltham, Massachusetts); and mounting media (Vector Labs, Burlingame, California).

Samples were fixed in 10% formalin and embedded in paraffin. Sections were rehydrated, and antigen retrieval was performed using a pressure cooker.[46] Following antigen retrieval, protein block was applied for 1 hour and slides washed with TBST. Slides were incubated with primary antibodies overnight at 2°C to 8°C, washed with TBST, incubated with secondary antibodies for 1 hour at room temperature, and washed with TBST. Sudan black solution (0.1% in alcohol) was applied to slides for 15 minutes to reduce auto-fluorescence. DAPI, used to stain cell nuclei, was applied for 10 minutes. Sections were washed with TBST, dehydrated, and mounted for imaging.

2.6 | Quantification of iNOS nuclear accumulation

iNOS production is expressed as the ratio of iNOS-containing cells to total (DAPI-labelled) cells. Sections were analysed using Nikon Ti-E-inverted fluorescence microscope. Images from five microscopic fields (20× magnification) were acquired. For each image, the total number of nuclei with iNOS nuclear fluorescence and the number of DAPI positive nuclei were manually counted. The percent of iNOS was calculated by dividing the number of nuclei exhibiting iNOS fluorescence by the total number of cells in each field by averaging the percentages from the five fields. Data are expressed as the mean ratio of iNOS nuclear accumulation $\pm$ SEM. For statistical analyses, data were transformed prior to post-hoc analyses.[47]

2.7 | Ethical considerations

All animal procedures were performed under approved University of California Irvine Institutional Animal Care and Use Committee animal protocols.

2.8 | Statistics

Data are presented as mean ± SEM. Our statistical analysis was performed with a two-tailed equal variance t-test. We compared the changes in Weber contrast in colour images for the closure of the wound, the changes in oxy haemoglobin, deoxyhaemoglobin, and StO2 between the non-diabetic and diabetic groups. We also compared the changes in iNOS production in the skin. Statistical significance was determined by ANOVA followed by post hoc analysis with Dunnett's test (a = 0.05).

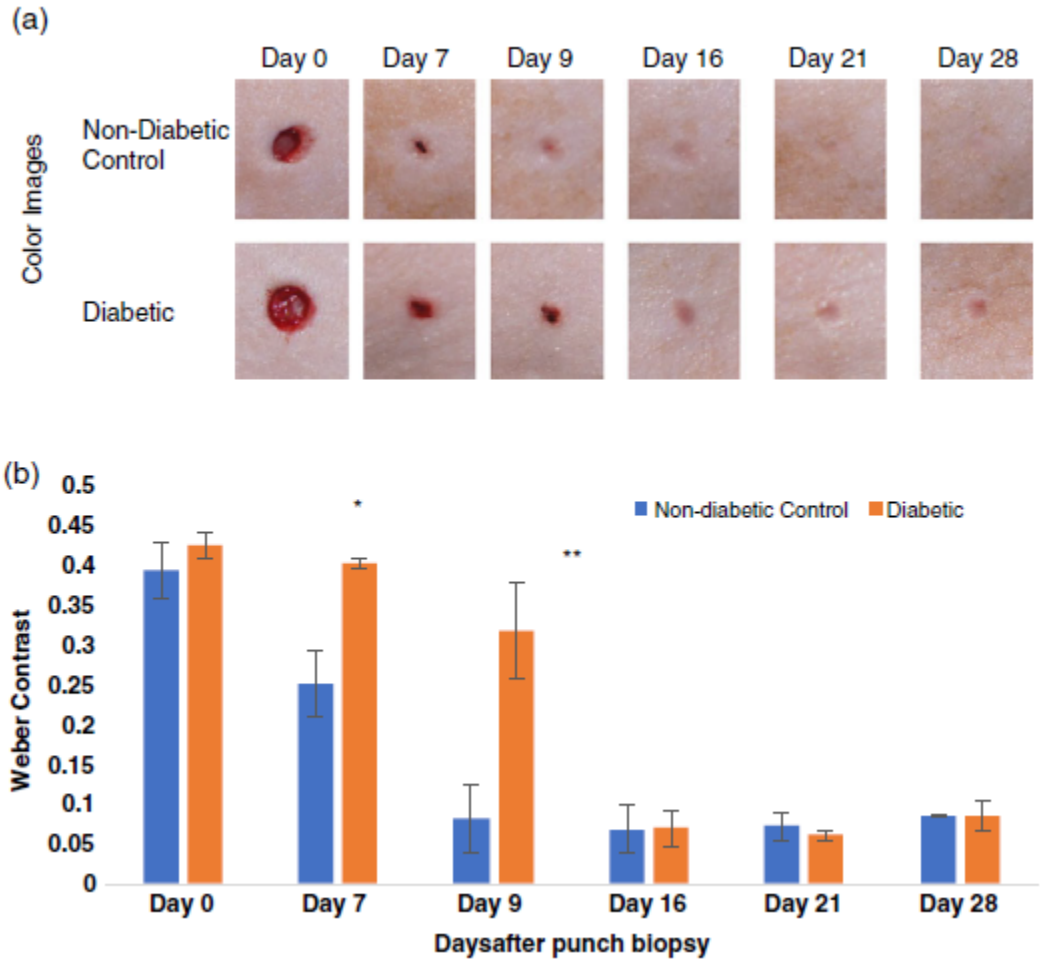

FIGURE 1 Colour images illustrating the longitudinal wound-healing process. A, Representative colour images of diabetic and non-diabetic control rats following the wound-healing process. The wound, which was created using a 4 mm round punch biopsy tool, was also 2 mm deep. In the non-diabetic group, the wound was closed after day 9, whereas in the diabetic group, the wound was closed after 21 days. B, Weber contrast, as the ratio of the change in intensity from the wounded site to non-wounded site, was calculated based on the colour images. The blue represents the non-diabetic

control rats (n = 3), and the orange represents the diabetic rats (n = 6). The healing process is delayed in the diabetic rats compared with the non-diabetic ones. These results were statistically significant for day 7 and day 9, where * represents $P < 0.05$ and ** represents $P < 0.01$ ANOVA. The error bars are mean $\pm$ SEM

3 | RESULTS

3.1 | Colour images and Weber contrast

Based on the colour images of non-diabetic control and diabetic rats, we observed that, in non-diabetic rats, wounds closed much more rapidly than in diabetic rats. Non-diabetic wounds were closed 7 days after the excision, and diabetic wounds closed by day 16 (Figure 1A). Weber contrast values (Figure 1B) showed a similar separation for nondiabetic wound and diabetic wounds. On day 0, when the wound was created, the values for the non-diabetic rats were 0.4 $\pm$ 0.0372 SEM and 0.42 $\pm$ SEM for the diabetic rats. On day 7, the separation became apparent as values for nondiabetic control rats reduced to 0.2 $\pm$ 0.04 SEM, whereas values for diabetic rats remained approximately the same at 0.4 $\pm$ 0.004 SEM. On day 9, the contrast values for the nondiabetic wounds were reduced to 0.08 $\pm$ 0.04 SEM, and the values for the diabetic wounds were 0.3 $\pm$ 0.05. By day 16, the quantitative values for both the groups were similar, approximately 0.06. Contrast values remained comparable until the end of the experiment.

3.2 | Oxyhaemoglobin (HbO2) values inside the wound

We used SFDI measurements to quantify and analyse the changes in HbO2 inside the wound during the healing process. Heat maps created by SFDI (Figure 2A) allowed us to quantify these changes. The HbO2 values for non-diabetic wounds at day 0 were 0.037 mM $\pm$ 0.001 SEM and 0.03 mM $\pm$ 0.005 SEM for diabetic wounds (Figure 2B). Seven days after wound creation, HbO2 values for nondiabetic wounds were reduced to 0.02 mM $\pm$ 0.002 SEM, and these values were significantly lower for the diabetic wounds, 0.018 mM $\pm$ 0.001 SEM. Nine days after the creation of wounds, values increased in the non-diabetic wounds to 0.03 mM $\pm$ 0.03 SEM and remained low for the diabetic wounds, 0.017 mM $\pm$ 0.001 SEM. Sixteen days after wound creation, there was a tendency for higher levels of HbO_2 inside non-diabetic wounds versus diabetic ones; however, this tendency was not statistically significant. HbO_2 values for diabetic and non-diabetic remained the same until the end of the experiment, approximately 0.02 mM ($P < 0.01$ by ANOVA across groups).

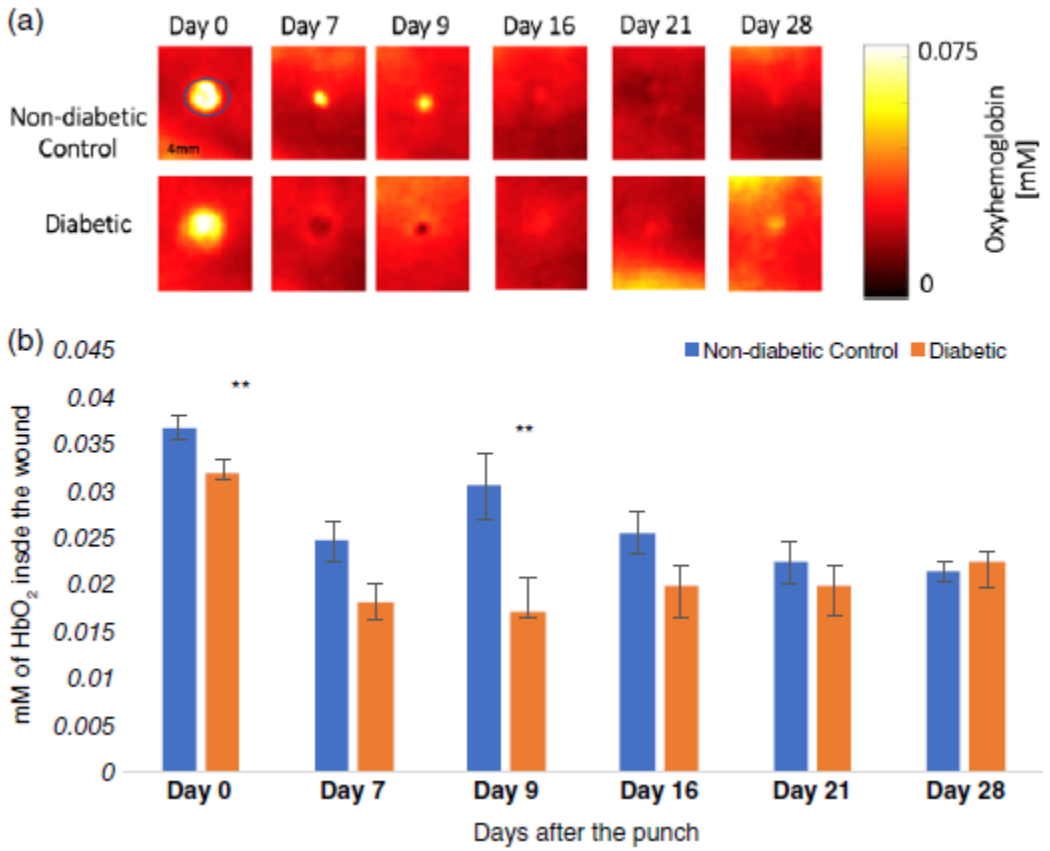

FIGURE 2 Comparison of oxyhaemoglobin concentration (HbO_2) levels in the wounded site in non-diabetic rats and diabetic rats. Wounds were created with 4 mm round punch biopsy tool (2 mm deep). A, Representative Spatial Frequency Domain Imaging (SFDI) maps of HbO_2 concentration. The yellower the colour, the higher the HbO2 concentration, and the darker (redder) colour represents lower HbO_2 levels. B, Quantification of oxyhaemoglobin (HbO_2) concentration inside the wound. The blue colour represents the non-diabetic control rats, and the orange colour represents the diabetic rats. This illustrates that the HbO_2 concentrations were reduced for the diabetic rats compared with control wounds on day 0 and at days 7 and 9. The concentration of HbO2 was restored once the wound was healed at day 28. The results were statistically significant for days 0 and 9, where ** represents $P < 0.0$

3.3 | Deoxyhaemoglobin (Hb) values inside the wound

We used SFDI to measure Hb concentration. Figure 3A illustrates higher levels of Hb inside the wound compared with the control wounds. In Figure 3B, we quantified these observations, indicating the tendency for higher Hb inside the wound in diabetic rats compared with controls. The Hb values for non-diabetic wounds were 0.016 mM $\pm$ 0.001 SEM and 0.014 mM $\pm$ 0.001 SEM for diabetic wounds. These values di not change for the non-diabetic wound for the rest of the experiment, but it increased in diabetic wounds. Seven days after wound creation, the Hb values for diabetic wounds increased to 0.2 mM

± 0.001 and remained high 9 days post-wound. The Hb values for diabetic wounds decreased only 16 days after wound creation to 0.14 mM ± 0.01, remaining constant until the experiment end. Throughout the experiment, there was a tendency for elevated Hb inside the diabetic wound region compared with non-diabetic wounds.

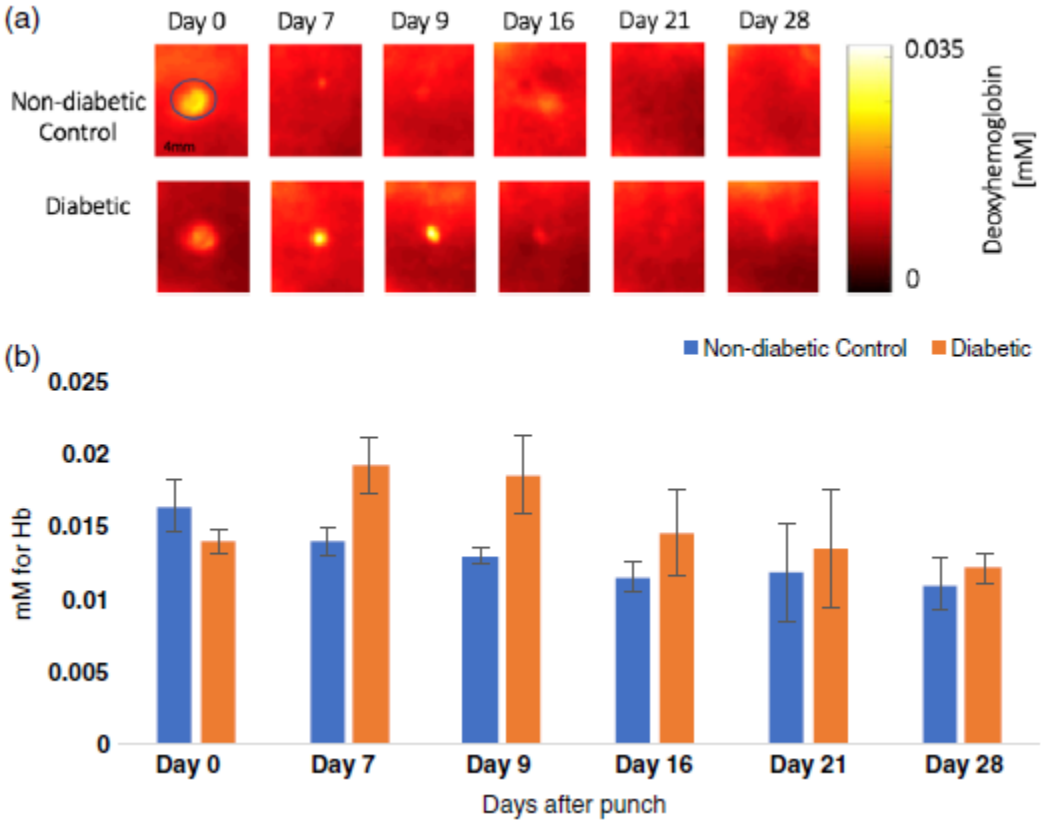

FIGURE 3 Spatial frequency domain imaging (SFDI) comparison of the deoxyhaemoglobin (Hb) concentration in the wounded site in non-diabetic rats and diabetic rats. A, Representative SFDI maps for evaluating the Hb levels. The yellower colour indicates higher Hb levels, and the darker (redder) colour represents lower Hb levels. B, Quantifying the changes in dexoxyhaemoglobin (Hb) concentration inside the wound in diabetic rats compared with nondiabetic rats. Blue represents the non-diabetic rats (n = 3), and orange represents the diabetic rats (n = 6). As can be seen, there is a tendency towards higher Hb concentrations in diabetic rat wounds compared with wounds in non-diabetic rats

3.4 | StO2 inside the wound

SFDI can also provide maps of tissue StO2. Figure 4A shows spatial maps of StO2, and in Figure 4B, the StO_2 for all wounds in each group, non-diabetic controls versus diabetic. At wound creation (day 0), the StO2 value for non-diabetic wounds was 0.69 ▯ 0.02 SEM, similar to the diabetic wounds 0.69 ± 0.01 SEM. Values did not change for nondiabetic wounds for the remainder of the experiment. As for the diabetic wounds, 7

days after wound creation, StO_2 values decreased to 0.48 ± 0.03 SEM. Values remained low in days 9 and 16 after wound creation: 0.49 ± 0.001 and 0.056 ± 0.001, respectively. StO_2 values increased only 21 days after the creation of the wound and became similar to the non-diabetic values through the remainder of the experiment.

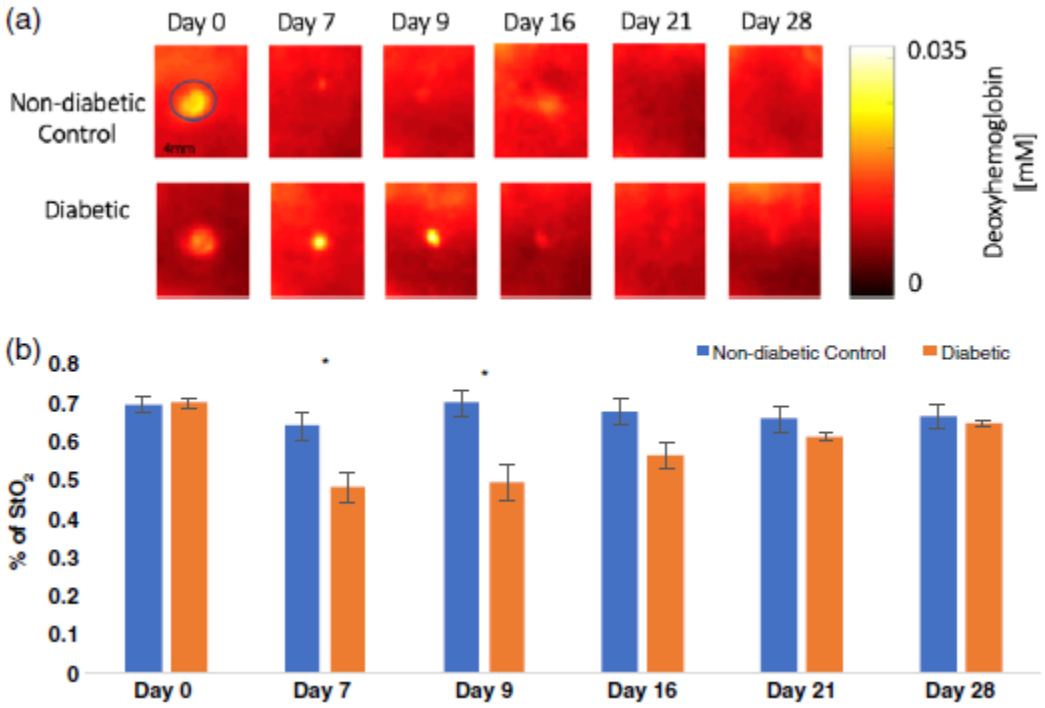

FIGURE 4 Spatial frequency domain imaging (SFDI) comparison of the oxygen saturation in the wounded area in the non-diabetic control and diabetic rats. A, Representative SFDI maps for evaluating oxygen saturation. The yellower colour indicates higher oxygen saturation levels, and the darker (redder) colour represents lower oxygen saturation. B, Time course of oxygen saturation values. The blue colour represents the non-diabetic control rats, and the orange colour represents the non-diabetic control rats. The oxygen saturation is reduced significantly at days 7 and 9 inside the wound for the diabetic rats, and this value is restored once the wounds are healed. The results were statistically significant when *P < 0.05. The error bars represent mean ± SEM

3.5 | Immunohistochemistry of accumulation of iNOS

Using iNOS antibody, the ratio of cell expression of iNOS was calculated based on co-localisation with nuclei stained with DAPI. In the non-diabetic control dermis, there was almost no evidence of iNOS expression (Figure 5); however, 28 days after STZ injection, most cells within the dermis expressed iNOS co-localised with DAPI. (Figure 5). This is indicative of higher oxidative stress levels and high inflammation because of hyperglycaemia. The ratio of iNOS to DAPI was 0.97 ± 0.024 in diabetic rats compared

with 0.3 ± 0.02 in non-diabetic rats. The results are statistically significant with P < 0.001.

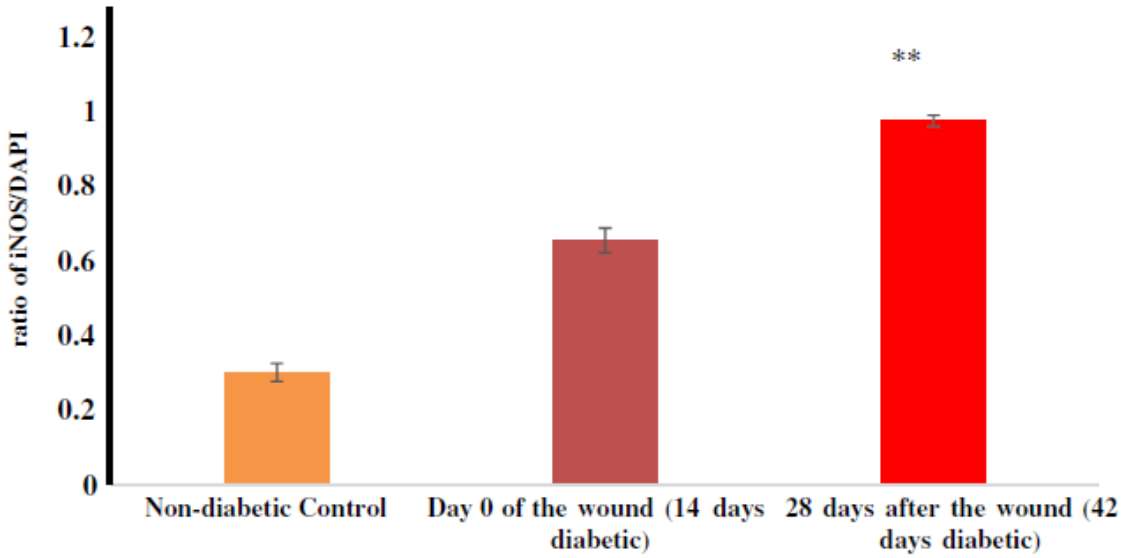

FIGURE 5 Expression, quantitative analysis of iNOS, and co-localisation with DAPI in the dermis of non-diabetic rats and diabetic rats at 14 and 28 days after induction of diabetes. The ratio iNOS/DAPI is an indicator of inflammation. Figure 5 Was made based on images from the skin of nondiabetic rats, from the skin of non-diabetic rats (n = 3 rats, 20 images), and 28 days after induction of diabetes (n = 6 rats, 20 images). There is almost no expression of iNOS in controls, and 14 days after the diabetic conditions, there is some expression of iNOS, and 28 days after diabetes induction, almost all of the cells inside the dermis are expressing iNOS. The images were taken with 20× magnification. Orange colour represents the non-diabetic control, the maroon colour represents 14 days after induction of diabetes, and the red represents 28 days after induction of diabetes. We evaluated the ratio between the DAPI-stained nucleus in the dermis to the iNOS that was produced in the dermis and co-localised with DAPI. There was a tendency for the higher production of iNOS after 14 days of diabetic conditions; however, this ratio was significantly higher 28 days after induction of diabetes. ** represents P < 0.01, and the error bars are mean ± SEM

4 | DISCUSSION

In this manuscript, we have discussed several methods that were used to evaluate diabetic wound healing and the changes occurring in the diabetic dermis that potentially lead to problems with delayed wound healing. Colour images and Weber contrast thresholding showed that wounds in diabetic rats healed at a slower rate than nondiabetic rats. To further understand the delay in wound healing, SFDI was used to evaluate changes in HbO_2, Hb, and StO_2.

SFDI results regarding Hb, HbO_2, and StO_2 inside the wound are consistent with other research on diabetic foot ulcers treated with hyperbaric oxygen therapy, which suggests that a lack of oxygen is a main cause for delayed and non-healing wounds in

diabetes.[48] Blood flow is compromised during diabetes because of damage to blood vessels and hyperglycaemia.[49] We showed that, after only 14 days (Figures 2–4), these changes can be observed using SFDI. Collectively, the results suggest that SFDI has the potential for predicting "at-risk" tissue associated with diabetes and may have applicability to non-healing foot ulcers. Non-invasive identification of regions of depressed StO2 and elevated Hb may enable physicians to better personalize appropriate therapy for each patient.

In addition to the macroscopic evaluation of wound healing, we also evaluated the changes in the skin, and especially in the dermis, regarding the inflammation , such as iNOS (Figures 5). In our study, we showed that, 14 days after hyperglycaemic onset, there is iNOS production at a level that continues to increase with time. Some level of iNOS is necessary for wound healing as knockout mice for iNOS showed impaired wound healing50; however, as shown in this study, overproduction of iNOS is also correlated with prolonged inflammation within the dermis and delays wound healing. As we mentioned earlier, HbO2 is a scavenger for NO and is one of the main pathways through which the body eliminates NO.[51] iNOS production is unregulated during hyperglycaemia and is associated with chronic inflammation during diabetes.[52] In the current study, we observed the changes and the complications of diabetes in relation to wound healing and inflammation by looking at the model of type I diabetes, which was induced by the injection of STZ. In order to make sure that our results are replicable and can be verified, there is a need to test this technology on additional models of diabetes. Future studies will look at additional models of diabetes such as type II diabetes in a larger sample size. In addition, in the current study, we showed that it is possible to predict non-healing diabetic wounds, one of the many complications of diabetes. Other complications of diabetes, such as neuropathy and ischaemia, play an extremely important part in clinical practice and should be considered in future studies as well. We suggest further investigation into these complications with the aim of predicting their onset with our technology, so it can be prevented with earlier treatments.

5 | CONCLUSION

About 15% to 25% of people with diabetes will develop a foot ulcer that is often resistant to healing; therefore, people with diabetes experience lower limb amputation at about 20 times the rate of non-diabetics.48 Understanding the changes that occur in diabetic dermis and within the wound itself using non-invasive methods such as SFDI has the potential for personalising treatment. In this study, we showed that HbO2 levels inside the diabetic wound are decreased, Hb levels are increased, and O2 saturation is decreased compared with wounds in normal control rats. This phenomenon, along with the over-production of dermis iNOS, causes chronic inflammation and delays the wound-healing process. Subsequently, we would develop the SFDI technology further to translate it to clinical setting.

ACKNOWLEDGEMENTS

This work was funded by NIH, including NIBIB P41EB015890 (A Biomedical Technology Resource), under which the human skin data were acquired. The content is

solely the responsibility of the authors and does not necessarily represent the official views of the NIBIB or NIH. In addition, this research is based on studies supported by the Air Force Office of Scientific Research under award number FA9550-14-1-0034 and FA9550-17-1-0193. Any opinions, findings, and conclusions or recommendations expressed in this material are those of the authors and do not necessarily reflect the views of the United States Air Force. We also thank the Arnold Beckman Foundation for their support in the completion of this research.

CONFLICTS OF INTEREST

Bruce Tromberg and Anthony Durkin are Co-Founders, Scientific Advisors, and Board Members of Modulated Imaging (MI), Inc.

ORCID

Mayer Saidian https://orcid.org/0000-0001-7511-4844

REFERENCES

1. Tankeu AT, Bigna JJ, Nansseu JR, et al. Global prevalence of diabetes mellitus in patients with tuberculosis: a systematic review and meta-analysis protocol. BMJ Open. 2017;7(6):e015170.
2. Reiber GE, Vileikyte L, Boyko EJ, et al. Causal pathways for incident lower-extremity ulcers in patients with diabetes from two settings. Diabetes Care. 1999;22(1):157-162.
3. Pemayun TG, Naibaho RM, Novitasari D, Amin N, Minuljo TT. Risk factors for lower extremity amputation in patients with diabetic foot ulcers: a hospital-based case-control study. Diabet Foot Ankle. 2015;6:29629.
4. Thomas Hess C. Checklist for factors affecting wound healing. Adv Skin Wound Care. 2011;24(4):192.
5. Ud-Din S, Bayat A. Non-invasive objective devices for monitoring the inflammatory, proliferative and remodelling phases of cutaneous wound healing and skin scarring. Exp Dermatol. 2016;25(8):579-585.
6. Shah JM, Omar E, Pai DR, Sood S. Cellular events and biomarkers of wound healing. Indian J Plast Surg. 2012;45(2):220-228.
7. Wu YS, Chen SN. Apoptotic cell: linkage of inflammation and wound healing. Front Pharmacol. 2014;5:1.
8. Lucas T, Waisman A, Ranjan R, et al. Differential roles of macrophages in diverse phases of skin repair. J Immunol. 2010;184(7):3964-3977.
9. Rodero MP, Khosrotehrani K. Skin wound healing modulation by macrophages. Int J Clin Exp Pathol. 2010;3(7):643-653.
10. Daley JM, Brancato SK, Thomay AA, Reichner JS, Albina JE. The phenotype of murine wound macrophages. J Leukoc Biol. 2010;87(1):59-67.
11. Schultz GS, Davidson JM, Kirsner RS, Bornstein P, Herman IM. Dynamic reciprocity in the wound microenvironment. Wound Repair Regen. 2011; 19(2):134-148.
12. Pierce GF. Inflammation in nonhealing diabetic wounds: the space-time continuum does matter. Am J Pathol. 2001;159(2):399-403.

13. Gerber RT, Holemans K, O'Brien-Coker I, et al. Increase of the isoprostane 8-isoprostaglandin f2alpha in maternal and fetal blood of rats with streptozotocin-induced diabetes: evidence of lipid peroxidation. Am J Obstet Gynecol. 2000;183(4):1035-1040.
14. Pautz A, Art J, Hahn S, Nowag S, Voss C, Kleinert H. Regulation of the expression of inducible nitric oxide synthase. Nitric Oxide. 2010;23(2): 75-93.
15. Yan SD, Schmidt AM, Anderson GM, et al. Enhanced cellular oxidant stress by the interaction of advanced glycation end products with their receptors/-binding proteins. J Biol Chem. 1994;269(13):9889-9897.
16. Aktan F. iNOS-mediated nitric oxide production and its regulation. Life Sci. 2004;75(6):639-653.
17. Neumann A, Schinzel R, Palm D, Riederer P, Munch G. High molecular weight hyaluronic acid inhibits advanced glycation endproduct-induced NF-kappaB activation and cytokine expression. FEBS Lett. 1999;453(3):283-287.
18. Mungrue IN, Husain M, Stewart DJ. The role of NOS in heart failure: lessons from murine genetic models. Heart Fail Rev. 2002;7(4):407-422.
19. Poon VK, Burd A. In vitro cytotoxity of silver: implication for clinical wound care. Burns. 2004;30(2):140-147.
20. Gordillo GM, Sen CK. Revisiting the essential role of oxygen in wound healing. Am J Surg. 2003;186(3):259-263.
21. Semenza GL. HIF-1 and human disease: one highly involved factor. Genes Dev. 2000;14(16):1983-1991.
22. Allen DB, Maguire JJ, Mahdavian M, et al. Wound hypoxia and acidosis limit neutrophil bacterial killing mechanisms. Arch Surg. 1997;132(9):991-996.
23. de Smet GHJ, Kroese LF, Menon AG, et al. Oxygen therapies and their effects on wound healing. Wound Repair Regen. 2017;25(4):591-608.
24. Algenstaedt P, Schaefer C, Biermann T, et al. Microvascular alterations in diabetic mice correlate with level of hyperglycemia. Diabetes. 2003;52(2):542-549.
25. Khaodhiar L, Dinh T, Schomacker KT, et al. The use of medical hyperspectral technology to evaluate microcirculatory changes in diabetic foot ulcers and to predict clinical outcomes. Diabetes Care. 2007;30(4):903-910.
26. Yudovsky D, Nouvong A, Schomacker K, Pilon L. Assessing diabetic foot ulcer development risk with hyperspectral tissue oximetry. J Biomed Opt. 2011;16(2):026009.
27. Ponticorvo A, Taydas E, Mazhar A, et al. Evaluating visual perception for assessing reconstructed flap health. J Surg Res. 2015;197(1):210-217.
28. Mazhar A, Sharif SA, Cuccia JD, Nelson JS, Kelly KM, Durkin AJ. Spatial frequency domain imaging of port wine stain biochemical composition in response to laser therapy: a pilot study. Lasers Surg Med. 2012;44(8): 611-621.
29. Nguyen JQ, Crouzet C, Mai T, et al. Spatial frequency domain imaging of burn wounds in a preclinical model of graded burn severity. J Biomed Opt. 2013;18(6):66010.
30. Ponticorvo A, Taydas E, Mazhar A, et al. Quantitative assessment of partial vascular occlusions in a swine pedicle flap model using spatial frequency domain imaging. Biomed Opt Express. 2013;4(2):298-306.
31. Ponticorvo A, Burmeister DM, Rowland R, et al. Quantitative long-term easurements of burns in a rat model using spatial frequency domain imaging (SFDI) and laser speckle imaging (LSI). Lasers Surg Med. 2017;49(3):293-304.

32. Masser DR, Otalora L, Clark NW, Kinter MT, Elliott MH, Freeman WM. Functional changes in the neural retina occur in the absence of mitochondrial dysfunction in a rodent model of diabetic retinopathy. J Neurochem. 2017; 143:595-608.
33. Dorsett-Martin WA. Rat models of skin wound healing: a review. Wound Repair Regen. 2004;12(6):591-599.
34. Peli E. Contrast in complex images. J Opt Soc Am A. 1990;7(10): 2032-2040.
35. Sprigle S, Zhang L, Duckworth M. Detection of skin erythema in darkly pigmented skin using multispectral images. Adv Skin Wound Care. 2009;22(4): 172-179.
36. Johnston ST, Simpson MJ, McElwain DL. How much information can be obtained from tracking the position of the leading edge in a scratch assay? J R Soc Interface. 2014;11(97):20140325.
37. Weszka JS. Survey of threshold selection techniques. Comput Vision Graph. 1978;7(2):259-265.
38. Yafi A, Vetter TS, Scholz T, et al. Postoperative quantitative assessment of reconstructive tissue status in a cutaneous flap model using spatial frequency domain imaging. Plast Reconstr Surg. 2011;127(1):117-130.
39. Nadeau KP, Ponticorvo A, Lee HJ, Lu D, Durkin AJ, Tromberg BJ. Quantitative assessment of renal arterial occlusion in a porcine model using spatial frequency domain imaging. Opt Lett. 2013;38(18):3566-3569.
40. Wilson RH, Crouzet C, Torabzadeh M, et al. High-speed spatial frequency domain imaging of rat cortex detects dynamic optical and physiological properties following cardiac arrest and resuscitation. Neurophotonics. 2017; 4(4):045008.
41. Cuccia DJ, Bevilacqua F, Durkin AJ, Ayers FR, Tromberg BJ. Quantitation and mapping of tissue optical properties using modulated imaging. J Biomed Opt. 2009;14(2):024012.
42. Torabzadeh M, Park IY, Bartels RA, Durkin AJ, Tromberg BJ. Compressed single pixel imaging in the spatial frequency domain. J Biomed Opt. 2017; 22(3):30501.
43. Ayers FR, Cuccia DJ, Kelly KM, Durkin AJ. Wide-field spatial mapping of in vivo tattoo skin optical properties using modulated imaging. Lasers Surg Med. 2009;41(6):442-453.
44. Saager RB, Quach A, Rowland RA, Baldado ML, Durkin AJ. Low-cost tissue simulating phantoms with adjustable wavelength-dependent scattering properties in the visible and infrared ranges. J Biomed Opt. 2016;21(6): 67001.
45. Erickson TA, Mazhar A, Cuccia D, Durkin AJ, Tunnell JW. Lookup-table method for imaging optical properties with structured illumination beyond the diffusion theory regime. J Biomed Opt. 2010;15(3):036013.
46. Pileri SA, Roncador G, Ceccarelli C, et al. Antigen retrieval techniques in immunohistochemistry: comparison of different methods. J Pathol. 1997; 183(1):116-123.
47. Hamby ME, Hewett JA, Hewett SJ. Smad3-dependent signaling underlies the TGF-beta1-mediated enhancement in astrocytic iNOS expression. Glia. 2010;58(11):1282-1291.
48. Health Quality Ontario. Hyperbaric oxygen therapy for the treatment of diabetic foot ulcers: a health technology assessment. Ont Health Technol Assess Ser. 2017;17(5):1-142.

49. Hashimoto R, Sugiyama T, Masahara H, Sakamoto M, Ubuka M, Maeno T. Impaired autoregulation of blood flow at the optic nerve head during vitrectomy in patients with type 2 diabetes. Am J Ophthalmol. 2017;181:125-133.
50. Kitano T, Yamada H, Kida M, Okada Y, Saika S, Yoshida M. Impaired healing of a cutaneous wound in an inducible nitric oxide synthase-knockout mouse. Dermatol Res Pract. 2017;2017:2184040.
51. Helms C, Kim-Shapiro DB. Hemoglobin-mediated nitric oxide signaling. Free Radic Biol Med. 2013;61:464-472.
52. Yang P, Cao Y, Li H. Hyperglycemia induces inducible nitric oxide synthase gene expression and consequent nitrosative stress via c-Jun N-terminal kinase activation. Am J Obstet Gynecol. 2010;203(2):185. e5-185.e111.

Funding information
Air Force Office of Scientific Research , Grant/Award Number: FA9550-14-1-0034 FA9550-17-1-0193; Center for Scientific Review, Grant/Award Number: NIBIB P41EB015890